Journal of Power Sources 261 (2014) 14–22

Contents lists available at ScienceDirect

Journal of Power Sources

journal homepage: www.elsevier.com/locate/jpowsour

Comparative degradation study of carbon supported proton exchange membrane fuel cell electrocatalysts – The influence of the platinum to carbon ratio on the degradation rate

Jozsef Speder [a,*], Alessandro Zana [a], Ioannis Spanos [a], Jacob J.K. Kirkensgaard [b], Kell Mortensen [b], Marianne Hanzlik [c], Matthias Arenz [a,*]

[a] Nano-Science Center, Department of Chemistry, University of Copenhagen, Universitetsparken 5, DK-2100 Copenhagen Ø, Denmark
[b] Niels Bohr Institute, University of Copenhagen, Universitetsparken 5, DK-2100 Copenhagen Ø, Denmark
[c] Technical University of Munich, Zentrum Elektronenmikroskopie, D-85747 Garching, Germany

HIGHLIGHTS

- Study of influence of Pt:C ratio on the degradation behaviour of Pt/C catalysts.
- Pt:C ratio influences degradation under start-up/shutdown conditions.
- Pt:C ratio has small influence on degradation under load cycles.
- Degradation on Vulcan XC72R substantial higher than on Ketjenblack EC-300.

GRAPHICAL ABSTRACT

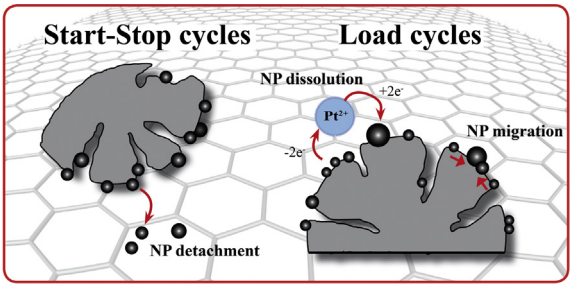

ARTICLE INFO

Article history:
Received 7 January 2014
Received in revised form
4 March 2014
Accepted 10 March 2014
Available online 20 March 2014

Keywords:
Colloidal toolbox synthesis
Proton exchange membrane fuel cells
Electrocatalyst durability
Degradation mechanisms
Carbon corrosion

ABSTRACT

A colloidal synthesis approach is used to prepare supported proton exchange membrane fuel cell (PEMFC) catalysts with various Pt loadings – from low to extremely high ones. The catalyst samples are used to continue our investigation of the role of the Pt:C ratio in the degradation processes. The influence of the platinum loading on the electrochemical surface area (ECSA) loss is evaluated in a systematic electrochemical study by using two commercially available carbon blacks, namely Vulcan XC72R and Ketjenblack EC-300J. Accelerated degradation tests simulating load cycle and start-up/shutdown conditions are carried out in accordance with the Fuel Cell Commercialization Conference of Japan (FCCJ) recommendations. Under conditions simulating the load cycle of PEM fuel cells no unambiguous correlation between the ECSA loss and the Pt:C ratio is found. By contrast, under conditions simulating the repetitive start-up/shutdown processes of PEMFCs the ECSA loss first increases with increasing Pt loading. However, it decreases again for very high loadings. Furthermore, the Vulcan samples exhibited higher ECSA losses than the Ketjenblack samples, indicating the important role of the physical and chemical properties of pristine carbon supports in the carbon degradation mechanism.

1. Introduction

A significant challenge for the commercial viability of proton exchange membrane fuel cells (PEMFCs) is the activity and stability [1–5] of the catalysts used for promoting the electrochemical energy conversion reactions. In the last years our research group

* Corresponding authors. Tel.: +45 35320002; fax: +45 35320214.
E-mail addresses: spederj@gmail.com (J. Speder), m.arenz@chem.ku.dk (M. Arenz).

http://dx.doi.org/10.1016/j.jpowsour.2014.03.039
0378-7753/

focussed on investigating the stability of catalysts. The chosen strategy was to apply measurements in electrochemical half-cells in order to enable fast and systematic assessments and to exclude the influence of "design" factors, for example the specific composition and preparation of the catalyst coated membrane (CCM). We introduced a specific investigation tool, dubbed identical location – transmission electron microscopy (IL-TEM), allowing for the first time at the nanoscale a direct comparison of same catalyst areas before and after treatment [6]. It could for example be shown that a specific commercial catalyst under the applied treatment conditions almost exclusively degraded via a particle detachment process [6,7]. In further studies of our and other groups the influence of parameters such as the carbon support or the Pt to carbon ratio on the stability of catalysts was investigated [8–12]. Comparing the degradation of different commercial catalysts, however, faced two drawbacks that inhibited truly systematic measurements. First, the absolute control over the synthesis, i.e. the ability to vary individual catalyst parameters (for example the Pt loading) while leaving others constant (for example the particle size and chemical state of the carbon support), was not given for commercial catalysts [12,13]. Additionally, the exact synthesis protocol of such samples is either not known or it is confidential. This drawback was mainly resolved by adapting a colloidal synthesis approach for the synthesis of the PEMFC catalysts [14]. The developed tool-box approach enables exactly this, selectively changing parameters like the Pt loading or the type of support material [15].

Second, a more systematic degradation treatment, i.e. standardized accelerated stress test (AST) conditions that are feasible for half-cell measurements (degradation treatments lasting several days are hardly feasible for half-cells) were needed. Such an AST treatment was recently proposed by the Fuel Cell Commercialization Conference of Japan (FCCJ) [16]. Two separate treatment conditions are recommended. One treatment simulates load cycle conditions, the second start-up/shutdown (Start–Stop) conditions of a PEMFC, thus enabling to investigate how specific operation conditions affect the degradation.

With both tools now at hand, truly systematic investigations of the degradation process of PEMFC catalysts are feasible, which hopefully amends a "material by design" approach for their development. In the presented study, we are focussing on the influence of the ratio between Pt and carbon on the degradation. In our recent work, we found that the measured electrochemical surface area (ECSA) loss in AST treatments strongly depends on the treatment conditions, i.e. treatments simulating load cycles and start-up/shutdown conditions [17]. These initial results are further investigated and complemented by careful microscopic (IL-TEM) as well as spectroscopic (small angle X-ray scattering; SAXS) investigations. Furthermore, the range of different Pt loadings (Pt to C ratios) was considerably extended revealing unexpected trends.

2. Experimental

2.1. Catalyst preparation

The investigated catalysts, hereafter called Pt/C, were synthesized in-house as described by Speder et al. [15]. The synthesis consists of two steps. First, a solution of colloidal Pt NPs with narrow size distribution of around 2 nm is prepared, then the NPs are deposited in varying amounts onto the high surface area (HSA) carbon support, i.e. Ketjenblack EC-300J (AkzoNobel, Brunauer–Emmett–Teller (BET) total surface area: 776 $m^2\ g^{-1}$, thereof 416 $m^2\ g^{-1}$ external (pores $>$ 2 nm) and 360 $m^2\ g^{-1}$ internal (pores $<$ 2 nm)), or Vulcan XC72R (Cabot Corporation, total BET area: 222 $m^2\ g^{-1}$, thereof 154 $m^2\ g^{-1}$ external and 68 $m^2\ g^{-1}$ internal [18]). Catalysts samples were prepared between 10 and 80 wt. % Pt. For a more detailed description of the Pt NP preparation the reader is referred to Refs. [14,15]. Briefly, a colloidal suspension of Pt NPs is synthesized by mixing under vigorous stirring 50 ml of a 0.4 M NaOH/ethylene glycol solution with a solution of 1.0 g $H_2PtCl_6 \cdot xH_2O$ dissolved in 50 ml ethylene glycol, in order to obtain a yellowish platinum hydroxide or oxide colloidal solution. The colloidal solution is then heated to 160 °C for 3 h to obtain a blackish-brown homogeneous metal particle colloidal suspension. The size and structure of the thus synthesized Pt NPs are controlled by transmission electron microscopy (TEM). The average diameter of the obtained Pt NPs is typically around 2 nm exhibiting a narrow size distribution. In order to support the Pt NPs onto an HSA carbon first 40 ml of HCl was added to the colloidal NP solution for precipitation. The solution was centrifuged (4000 rpm, 6 min) and repeatedly washed with 1 M HCl before dispersing it in acetone. The as-synthesized Pt NPs were deposited onto different HSA carbons by mixing the NP suspension with carbon black in 3 ml of acetone and sonicating for 1 h. Finally the catalyst was dried.

The Pt loading of the catalysts was confirmed by using inductively coupled plasma mass spectrometry (ICP-MS) measurements. For this, the catalysts were dissolved in inverse aqua regia (freshly mixed cc. HNO_3 and cc. HCl in a volumetric ratio of 3:1, respectively). The concentration of platinum in the diluted aqua regia solution was analyzed by ICP-MS (NexION 300X, Perkin Elmer) through a Meinhard quartz nebulizer and a cyclonic spray chamber, operating at nebulizer gas flow rates of between 1.0 and 1.02 L min^{-1} (Ar, purity 5.0).

2.2. Electrochemical characterization

The electrochemical measurements were performed in an all-Teflon three-compartment electrochemical cell [19], using a home-built multi-electrode setup with eight glassy carbon (GC) tips used as working electrodes (WE). The potential was controlled using a potentiostat (*Princeton* Applied Research, model *263A*) in a three electrode setup. The counter (auxiliary) electrode was a carbon rod, the reference electrode a Schott Ag/AgCl/KCl(sat.) electrode located in a second compartment separated by a membrane (Nafion®) in order to avoid the diffusion of Cl^- ions into the main compartment [20]. All potentials, however, are referred to the reversible hydrogen electrode (RHE) potential, which was experimentally determined for each measurement series. All acid solutions were prepared from Millipore® water (>18.3 MΩ cm, *Total Oxidizable Carbon*, TOC $<$ 5 ppb) and Suprapur acids (Merck). The measurements were performed at room temperature. Prior to the RDE measurements the glassy carbon (GC) working electrode (5 mm diameter, 0.196 cm^2 geometrical surface area) was polished to mirror finish using alumina oxide paste, 0.3 and 0.05 μm (Buehler-Met, de-agglomerated α-alumina and γ-alumina, respectively), and cleaned ultrasonically in ultrapure water and cc. 70% $HClO_4$. The catalyst ink was prepared by mixing the catalyst powder with ultrapure water to a concentration of 0.14 $mg_{Pt}\ cm^{-3}$ and ultrasonically dispersing the suspension for 30 min. Before applying the catalyst ink to the GC electrode the suspension was ultrasonically dispersed for an additional 5 min. Then a volume of 20 μL of the suspension was pipetted onto the GC electrode leading to a Pt loading of 14 $\mu g_{Pt}\ cm^{-2}$ and thereafter dried in a nitrogen gas stream. Care should be taken that the catalyst ink is not heated from the ultrasonic bath, to avoid errors from changing water density. All electrochemical experiments were performed in 0.1 M $HClO_4$ solution. Prior to the measurements the electrolyte was de-aerated by purging with Ar gas (*99.998%, Air Liquide*), and the measurements were started with cleaning the catalyst by potential cycles between 0.05 and 1.0 V_{RHE} at a scan rate of 50 mV s^{-1}. For the measurement of the RHE the electrolyte (0.1 M $HClO_4$) was purged with hydrogen

(*Alphagaz 1*, *Air Liquide*) and the RHE was determined from an RDE polarization curve. The electrochemically accessible surface area (ECSA) of the catalysts was determined from the CO stripping charge [21] recorded at a sweep rate of 50 mV s^{-1} in a multi-electrode configuration.

2.3. Accelerated stress test (AST) protocols

The degradation behaviour of catalyst was evaluated employing two degradation treatments in accordance with the FCCJ recommendations [16]. One treatment simulates load cycle conditions experienced in a fuel cell stack in actual fuel cell vehicles and consisted of applying square-wave potential steps between 0.6 and 1.0 V_{RHE} with a rest time of 3 s at each potential. The total treatment lasted 9000 cycles (15 h). The ECSA is measured by CO stripping and it is periodically monitored at every 600 cycles up to 3000 potential cycles and then at 6000 and 9000 potential cycles. The second treatment simulates start-up/shutdown conditions and consisted of potential cycling between 1 and 1.5 V_{RHE} with a sweep rate of 500 mV s^{-1}. This treatment is used to simulate start-up operations conditions when the H_2 gas in the anode flowfield is gradually replaced for air, and therefore, cathode can experience high potential ca. 1.4 V_{RHE} [22]. It is also assumed that when hydrogen is introduced to the anode flowfield, the cathode potential behaviour shows a triangular change [23]. The total treatment lasted 27,000 potential cycles (15 h). The ECSA is characterized at every 1800 cycles up to 9000 potential cycles and then at 18,000 and 27,000 potential cycles. All the measurements were conducted at room temperature in Ar saturated 0.1 M $HClO_4$ and without rotation. For more details on treatments, the reader is referred to the FCCJ protocol in Refs. [16,24].

2.4. Identical location transmission electron microscopy (IL-TEM)

In order to study the particle size of the NPs and their distribution on the carbon support TEM micrographs of the as-prepared catalysts were recorded with a Tecnai T20 G2 S-TEM at 200 kV. For the IL-TEM investigations the catalyst suspension was diluted by a factor of 1:10. 5 ml of catalyst suspension were pipetted onto a gold finder grid (400 mesh; Plano, Germany) coated with an amorphous carbon film. In order to keep the catalyst loading as low as possible (to avoid overlapping of catalyst particles), the drop was delicately absorbed off the grid after approximately 10 s using a tissue. The grid was dried, and then investigated using a JEM 2010 (JEOL, Japan) with an accelerating voltage of 120 kV. TEM micrographs were recorded before and after the treatment procedures.

2.5. Small angle X-ray scattering (SAXS)

The platinum particle size distribution of the supported catalysts were determined by Small Angle X-ray Scattering (SAXS) using a SAXSLab instrument (JJ-X-ray, Denmark) equipped with a Rigaku 100XL+ micro focus sealed X-ray tube and a Dectris 2D 300 K Pilatus detector. On this instrument the detector is moveable allowing different structural length scales to be accessed. Here the magnitude of the scattering vector is defined as $q = 4\pi/\lambda\sin(\theta)$ with λ being the X-ray wavelength and θ half of the scattering angle. Samples were sealed between two 5–7 μm thick mica windows and measurements were performed *in vacuo*. The data analysis follows Ref. [25] with small modifications. The scattering data are fitted to the following expression:

$$I(q) = C_1 I_{CARBON}(q) + C_2 + C_3 \Pi(q) + C_4 \int P_S^2(q,R) D(R) \mathrm{d}R \quad (1)$$

where C_i are constants and the four terms represent the background from the pure carbon support with no platinum loaded, a small constant background, a term accounting for the pore structure and a term representing the platinum particles, respectively. The I_{CARBON}-term, representing the carbon background can be measured directly for the untreated samples, however, this is more difficult for the treated samples since the presence of the platinum influences the degradation structure of the carbon. In those cases we follow Ref. [17] and model the pure carbon as a power law q^n, where exponent n comes out from the fit as ca. 3.3 in accordance with Ref. [17]. The $\Pi(q)$-pore term is given by the Lorentz expression:

$$\Pi(q) = \frac{a^4}{\left(1 + a^2 q^2\right)^2} \quad (2)$$

with a being a characteristic pore dimension. The final term, the sphere term representing the platinum particles is described by a lognormal size distribution of spherical particles. The form factor amplitude of a sphere with radius R is given by

$$P_S(q,R) = 4\pi R^3 \frac{\sin qR - qR\cos qR}{(qR)^3} \quad (3)$$

and the lognormal size distribution by

$$D(R) = \frac{1}{R\sigma\sqrt{2\pi}} \exp\left(\frac{-[\ln(R/R_0)]^2}{2\sigma^2}\right) \quad (4)$$

where σ is the variance and R_0 the geometric mean of the lognormal distribution. From each particle size distribution $D(R)$, we calculated a volume normalized surface area of each catalyst by using the following equation:

$$\frac{A}{V} = \frac{\sum_i D(R_i) 4\pi R_i^2}{\sum_i D(R_i) \frac{4\pi}{3} R_i^3} \quad (5)$$

Assuming mass is proportional to volume the ratios of these areas are directly compared to the ratios of the ECSA. Further, by dividing this ratio with the platinum density of 21.45 g cm^{-3} absolute numbers per unit mass can be obtained for each sample. The presented model fits are computed using home-written MATLAB code.

3. Results and discussion

As discussed in the Introduction, the presented work focuses on the influence of the ratio between Pt and carbon on the degradation. Employing a toolbox synthesis approach [15], we were able to cover a broad range of catalysts consisting of Pt NPs from the same base suspension, but supported with different loadings on Vulcan XC72R and Ketjenblack EC-300J carbon supports, respectively.

3.1. PEM fuel cell electrocatalysts supported on high surface area carbon supports with varying metal loadings

In Fig. 1 the properties of the series of catalysts are summarized. The electrochemical surface area of the samples is plotted as a function of the nominal Pt content expressed in wt. %. As seen the ECSA of the samples stays constant over a wide Pt loading range. That is, using the colloidal synthesis approach the Pt loading can be varied from 10 to up to more than 70 wt. % without inducing

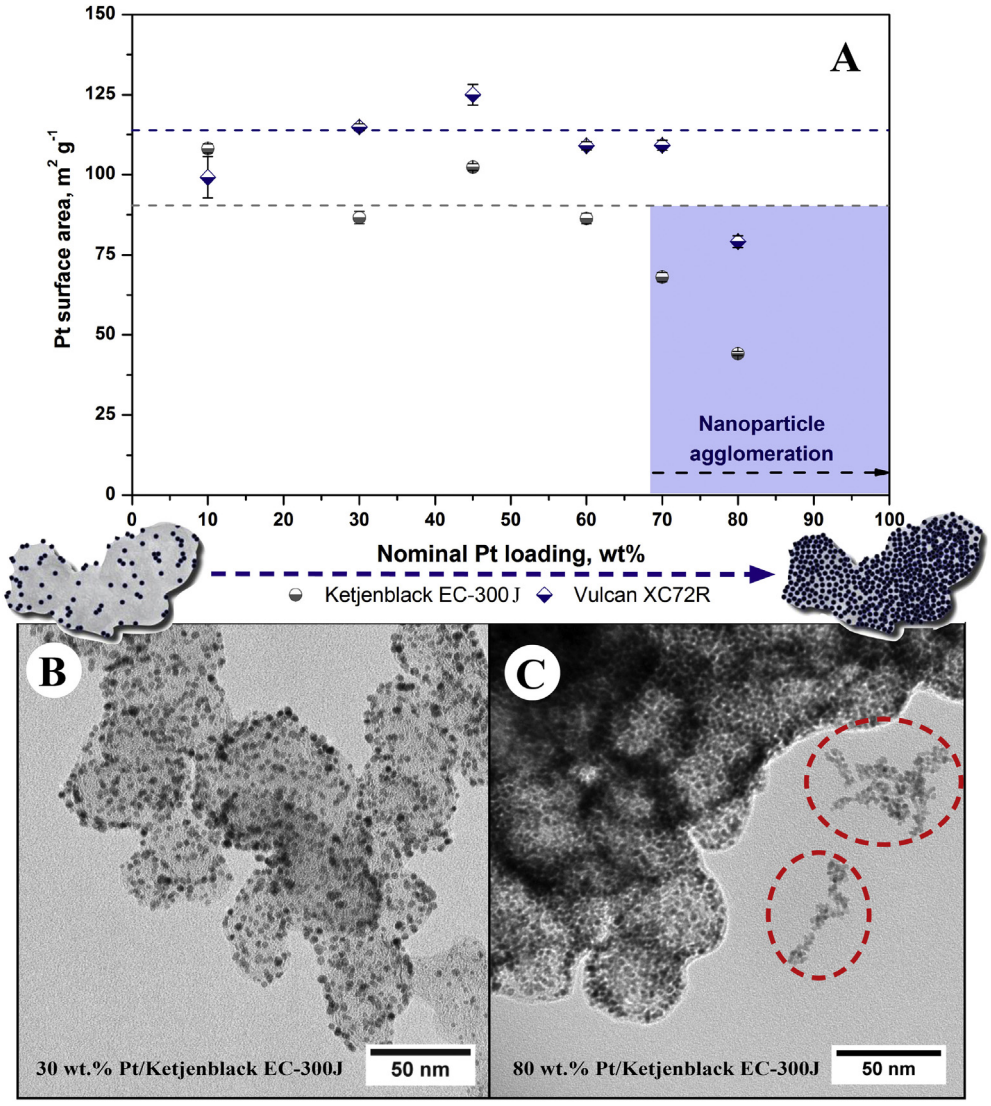

Fig. 1. Comparison of Pt/Ketjenblack and Pt/Vulcan catalysts. In (A) the ECSA calculated from CO stripping measurements and the respective measured (using ICP-MS) Pt content is shown as a function of the nominal Pt content expressed in wt. % (only slight differences between nominal and measured Pt content occur). In the lower part representative TEM micrographs of the synthesized catalysts are shown for (B) 30 wt. % and (C) 80 wt. % Pt/Ketjenblack catalysts. In (C) unsupported Pt NPs are marked by red circles. (For interpretation of the references to colour in this figure legend, the reader is referred to the web version of this article.)

particle agglomeration. Furthermore, the difference between experimental and nominal Pt content was between 10 and 20% in all samples (the lower values were obtained for high Pt loading) proving that the colloidal toolbox synthesis approach enables an effective and simple way of attachment of Pt NPs to different carbon supports. Only at extreme high loadings where the packing density of the Pt NPs on the carbon support is maximized, the NPs start to agglomerate and unsupported NPs are detected (see representative TEM micrograph in Fig. 1C). As a consequence the ECSA of these samples decreases.

A further interesting observation is that in general on the Vulcan support higher ECSA values are achieved compared to EC-300J, indicating a higher degree of dispersion and utilization of the colloidal Pt NPs (the exception for the samples with 10 wt. % Pt loading on carbon for which within the error the same ECSA was determined can be explained by fact that such samples are more difficult to measure due to the thicker catalysts layer). In the literature, Pt dispersion on high surface area carbons is often correlated with the BET surface area of the support [26–29]. With 776 $m^2\ g^{-1}$ vs. 222 $m^2\ g^{-1}$, the BET surface area of EC-300J, however, is considerably higher than that of Vulcan XC72R [30,31]. Even taking into account that part of the total BET surface area consists of micropores <2 nm and thus is not available for NPs adhesion does not change the picture. The external surface area of EC-300J is 416 $m^2\ g^{-1}$ and therefore still considerably larger than the 154 $m^2\ g^{-1}$ of Vulcan XC72R.

The consistently higher ECSA values on Vulcan are therefore somewhat surprising, indicating that using a colloidal synthesis approach the metal dispersion on carbon blacks strongly depends on defect sites and chemical species present on carbon surfaces. Oxygen based functional groups such as quinones (>C═O), hydroxyl and/or phenols (−OH), and carboxyl (−COOH), are reported to increase Pt NP dispersion by serving as adsorption sites [32]. As it has previously shown [33,34] the Vulcan support exhibits a larger number of defect sites, which enables a better and more homogenous Pt dispersion. Furthermore, the pore structure of Ketjenblack may lead to an encapsulation of some Pt NPs so that they become inaccessible [35].

3.2. Accelerated stress (AST) tests

In the following the electrocatalysts were subjected to degradation tests based on the FCCJ recommendations [16]. We chose these degradation test protocols because the treatment time can be limited (15 h) and carbon corrosion and Pt NP growth can be investigated separately [36]. The results are summarized in Fig. 2.

It is seen that simulating load cycles (potential steps between 0.6 and 1.0 V_{RHE} with a holding time of 3:3 s) the ECSA loss after 15 h treatment time is between 35 and 45%. No clear dependence on either the carbon support or the Pt loading is detected. Such behaviour is in line with the proposition that Pt dissolution plays an important role in the degradation upon such treatment (see also discussion below) [37]. These results are in contrast to the findings applying AST treatments simulating start-up/shutdown conditions (cycling between 1.0 and 1.5 V_{RHE} with a sweep rate of 500 mV s^{-1}) summarized in Fig. 2B. As reported previously, under such conditions the observed ECSA loss strongly depends on the high surface area carbon support [17]. The catalysts using Vulcan as support exhibit significantly higher losses than the catalysts using Ketjenblack as support. For example, after 15 h AST treatment simulating start-up/shutdown conditions the ECSA loss of 30 wt. % Pt/Vulcan is roughly twice as high as for 30 wt. % Pt/Ketjenblack. We interpret this result such that Vulcan exhibits a higher density of surface defects (edges and corners of basal planes) where carbon corrosion is initiated due to unsaturated valences and free electron density [38]. Our results are in contrast to reports proposing that the corrosion rate of carbon depends linearly on its BET surface area, i.e. that the carbon corrosion rates normalized by BET surface area are similar for Ketjenblack and Vulcan [39,40].

Our new data concerning highly loaded samples show an additional and rather surprising trend. Systematically increasing the Pt loading of the catalysts from 10 to 80 wt. %, at first the ECSA loss increases with increasing Pt loading; the ECSA of highly loaded

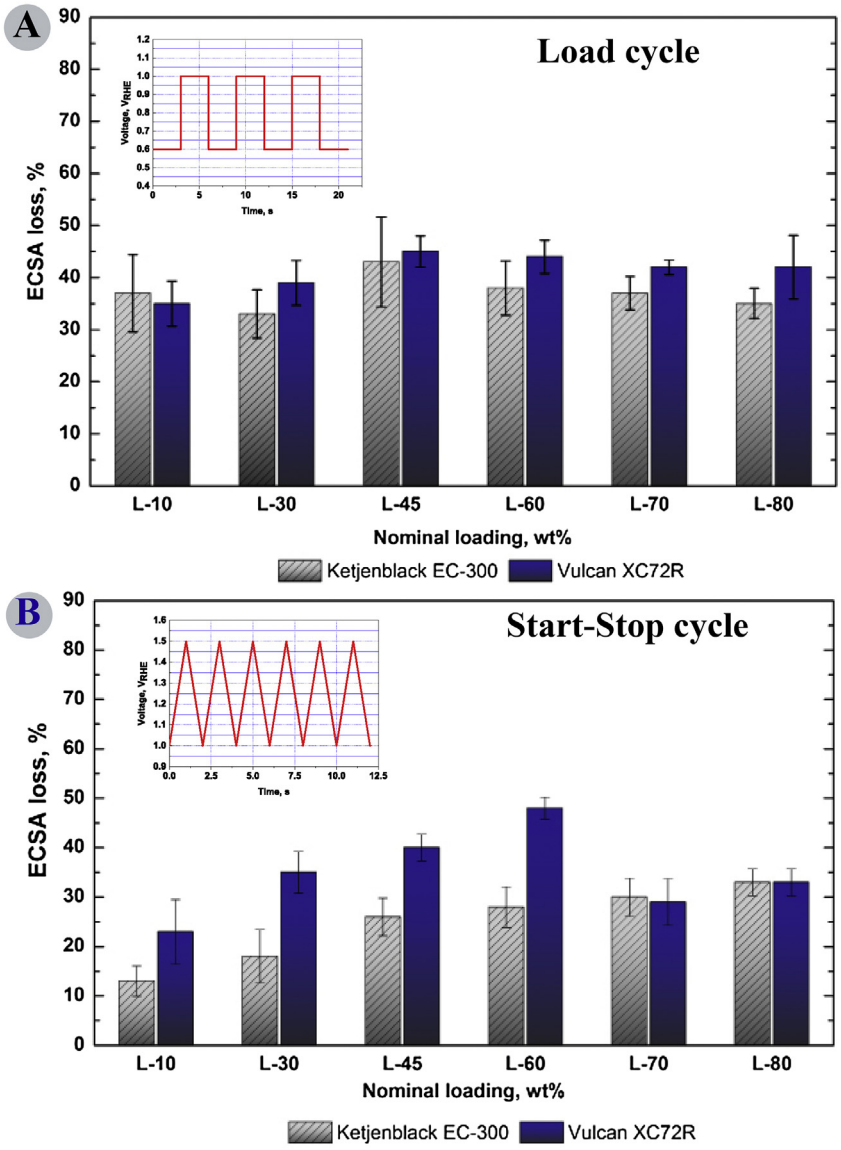

Fig. 2. Summary of the determined ECSA loss for Pt/Ketjenblack and Pt/Vulcan as function of Pt loading. In (A) the catalysts were subjected to potential steps between 0.6 and 1.0 V_{RHE} with a holding time of 3:3 s (simulating load cycles) for 9000 cycles. In (B) the catalysts were treated by potential cycling between 1.0 and 1.5 V_{RHE} with a sweep rate of 500 mV s^{-1} (simulating Start–Stop cycles) for 27,000 cycles. All measurements were conducted in 0.1 M $HClO_4$ electrolyte and at room temperature. The corresponding cycle profiles are sketched in the insets.

Vulcan catalysts (Pt wt. % ≥ 70), however, decrease again. Furthermore, for such highly loaded catalysts no difference in ECSA loss between the two high surface area carbons is seen. At high loadings, essentially the catalysts behave more like a Pt film than a typical PEMFC catalyst containing Pt NPs. Comparing the ECSA loss with the initial ECSA value (Fig. 1), indicates that the "Pt film behaviour" sets in once the carbon flakes of the support are entirely covered by Pt NPs, just before the ECSA starts to drop. In other words, if the carbon flakes are entirely covered by Pt NPs the nanoparticle film acts as protection layer for the carbon degradation.

3.3. Small angle X-ray scattering (SAXS)

In order to gain a better understanding of the differences between the catalysts supported on Vulcan and those supported on Ketjenblack, the electrochemical measurements were combined with SAXS and IL-TEM measurements. The SAXS technique provides an integral (of the whole sample) overview of the changes in particle size distribution upon treatment, whereas with IL-TEM local phenomena are probed locally on the nanoscale.

In Fig. 3 the initial and final particle size distributions (after 15 h AST treatment) of a Pt/Vulcan and Pt/Ketjenblack catalyst with 30 wt. % Pt loading are shown. The insets display the change of the average particle size with time during simulation of start-up/shutdown conditions. In addition all key data are summarized in Table 1. The SAXS data indicate an average particle size of 1.7 ± 1.2 nm (FWHM as error) for the pristine Pt/Vulcan sample and 2.0 ± 1.6 nm for Pt/Ketjenblack. The corresponding Pt surface area of the Pt/Vulcan and Pt/Ketjenblack samples calculated from the SAXS data, using the Eq. (5) are 126.5 and 93.9 $m^2\ g^{-1}$. These numbers are in excellent agreement with the measured electrochemical surface area (ECSA) data of Pt/Vulcan i.e. 111 ± 1.0 $m^2\ g^{-1}$, and Pt/Ketjenblack, i.e. 80 ± 1.9 $m^2\ g^{-1}$ taking into account that not the complete NP surface is electrochemically assessable (as assumed in the calculation from the SAXS data), but parts of it are covered by the carbon support.

Upon applying AST treatments the particle size distribution considerably changes, i.e. the average particle size increases as expected. The SAXS data show that the resulting shape of the distribution function depends on the treatment conditions. However, no considerable differences between the two catalysts supports, Ketjenblack and Vulcan, are observed. Upon applying conditions simulating Start–Stop processes in PEMFC, the average particle size increases, but the shape of the distribution function and the full width of half maximum (FWHM) stay the same as the one of the pristine samples or only change slightly in case of the Vulcan support. Such behaviour is in line with a particle detachment process, where smaller particles exhibit a slightly higher likelihood of detachment than larger ones (see also the IL-TEM data discussed below). Simulating load cycle conditions results in somewhat larger changes in the average particle size. Most important, in addition to the average particle size the shape of the distribution function changes as well. This is also reflected by the concomitant significant change in FWHM observed on both carbon supports. The results unambiguously demonstrate that the degradation mechanisms under Start–Stop and load cycle conditions are considerably different. The changes in the particle size distribution function upon simulating load cycles, are in agreement with Pt NP growth via electrochemical Oswald ripening as well as migration coalescence [41]. The electrochemical Ostwald ripening takes place when small Pt NPs dissolve, diffuse, and redeposit onto previously existing larger NPs in order to minimize their surface energy. Particle coalescence via migration occurs when Pt particles are in close proximity and sinter together to form larger particles. Both mechanisms lead to a considerable increase of the average particle size accompanied by a change in the FWHM of the distribution function, i.e. a shift of the typical Gaussian particle size distribution to higher and broader size distributions (increase of the FWHM).

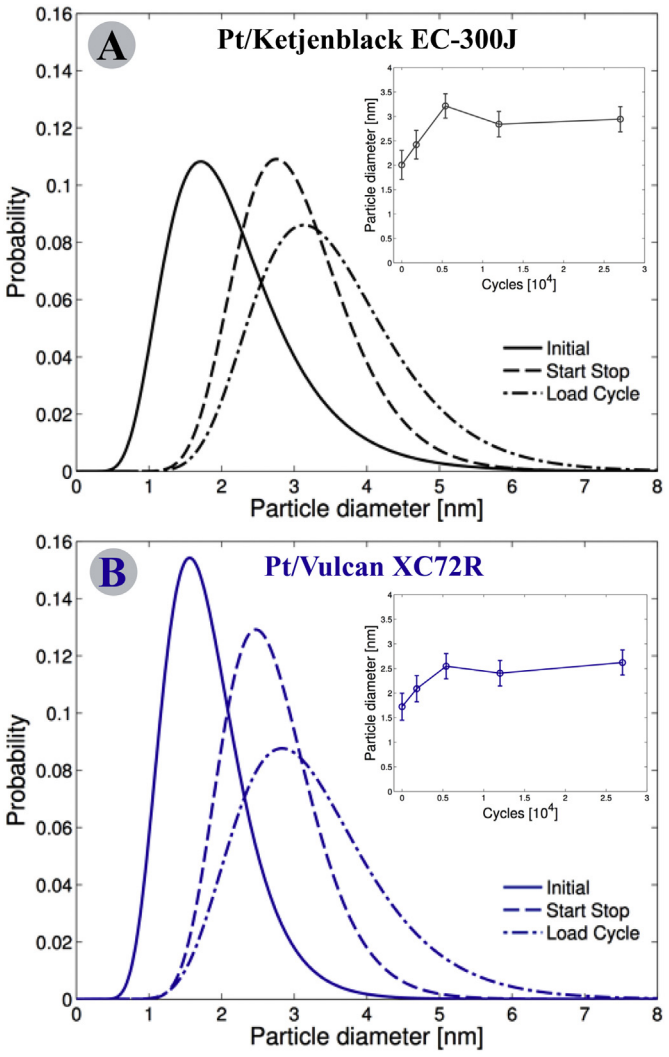

Fig. 3. SAXS data for 30 wt. % Pt/Ketjenblack (A) and Pt/Vulcan (B) cycled between 1.0 and 1.5 V_{RHE} with a sweep rate of 500 mV s^{-1} for 27,000 cycles (15 h) and between 0.6 and 1.0 V_{RHE} with a holding potential of 3:3 s for 9000 cycles (15 h) in 0.1 M $HClO_4$. The insets show the evolution of the average Pt NP size during Start–Stop cycling condition.

Table 1
Influence of the AST tests on the average Pt NP size and ECSA of 30 wt. % Pt/Ketjenblack and Pt/Vulcan samples.

	NP radius (nm)[a]	FWHM (nm)	ECSA ($m^2\ g^{-1}$)[b]	ECSA ($m^2\ g^{-1}$)[c]
Pt/Ketjenblack EC-300J				
Initial	1.00	0.83	93.9	80
Start–Stop	1.50	0.81	80.6 (14% loss)	65 (18% loss)
Load cycle	1.70	1.07	67.3 (28% loss)	53 (33% loss)
Pt/Vulcan XC72R				
Initial	0.86	0.59	126.5	111
Start–Stop	1.32	0.71	92 (27% loss)	68 (38% loss)
Load cycle	1.57	1.06	70.2 (44% loss)	65 (41% loss)

[a] Determined by fitting experimental SAXS curves via Eqs. (1)–(4).
[b] Derived from the NP radius via Eq. (5) assuming spherical particles.
[c] Determined from CO stripping.

3.4. Identical-location transmission electron microscopy (IL-TEM)

In order to examine the degradation process also on a microscopic scale, IL-TEM measurements were performed. As in the SAXS data no considerable differences in the main degradation mechanisms were observed, we concentrate on the samples using Ketjenblack as support. Corresponding observations were made on the Pt/Vulcan samples.

The IL-TEM data are displayed in Fig. 4. In accordance with the observed ECSA loss observed, the TEM micrographs of identical locations of the catalyst before and after potential cycling demonstrate that the accelerated degradation treatment results in a considerable reduction in the amount of Pt nanoparticles on the carbon support.

Upon the AST treatment simulating Start–Stop conditions (Fig. 4A and B), a particle detachment mechanism is observed. This result is in agreement with previous studies on different catalysts and to fact that after the AST treatment unsupported Pt NPs are observed on the carbon film of the Au grid (not shown) [36]. Such a mechanism is most likely a result of carbon corrosion, partial or complete, destabilizing the anchor sites for the Pt NPs. However, the IL-TEM micrographs also show individual Pt agglomerates (marked by the red circles in the web version in Fig. 4B), indicating that under such conditions coalescence occurs as well. Due to the limited growth observed in SAXS, this process, however, is not considered to be the major degradation process. Furthermore, some of the agglomerates might indeed be gold deposits formed from the dissolution–redeposition of Au from the TEM grid. We indicate this are by green circle in Fig. 4B. It should be noted that during preparation of the SAXS samples, no gold was present in the electrochemical cell and thus no such process can occur.

Upon simulating load cycle conditions, Fig. 4C and D, no unsupported NPs were observed on the carbon film of the TEM grid. Thus no massive particle detachment occurs. Instead, and in line with the SAXS data the particle growth is more pronounced. If the observed particle growth is mainly due to migration and coalescence or due to electrochemical Oswald ripening cannot be clearly identified. Signs of both processes are seen from the shape of the resulting Pt NPs, i.e. some are round as expected in electrochemical Oswald ripening, some dendritic as expected in migration and coalescence.

4. Conclusions

We demonstrate how a colloidal synthesis approach can be used to systematically investigate high surface area carbon supported catalysts for PEMFCs using AST in half-cells. Our data clearly show that the loss in ECSA due to AST treatments simulating Start–Stop conditions depends on the carbon support as well as on Pt loading. By contrast, simulating load cycle conditions no unambiguous

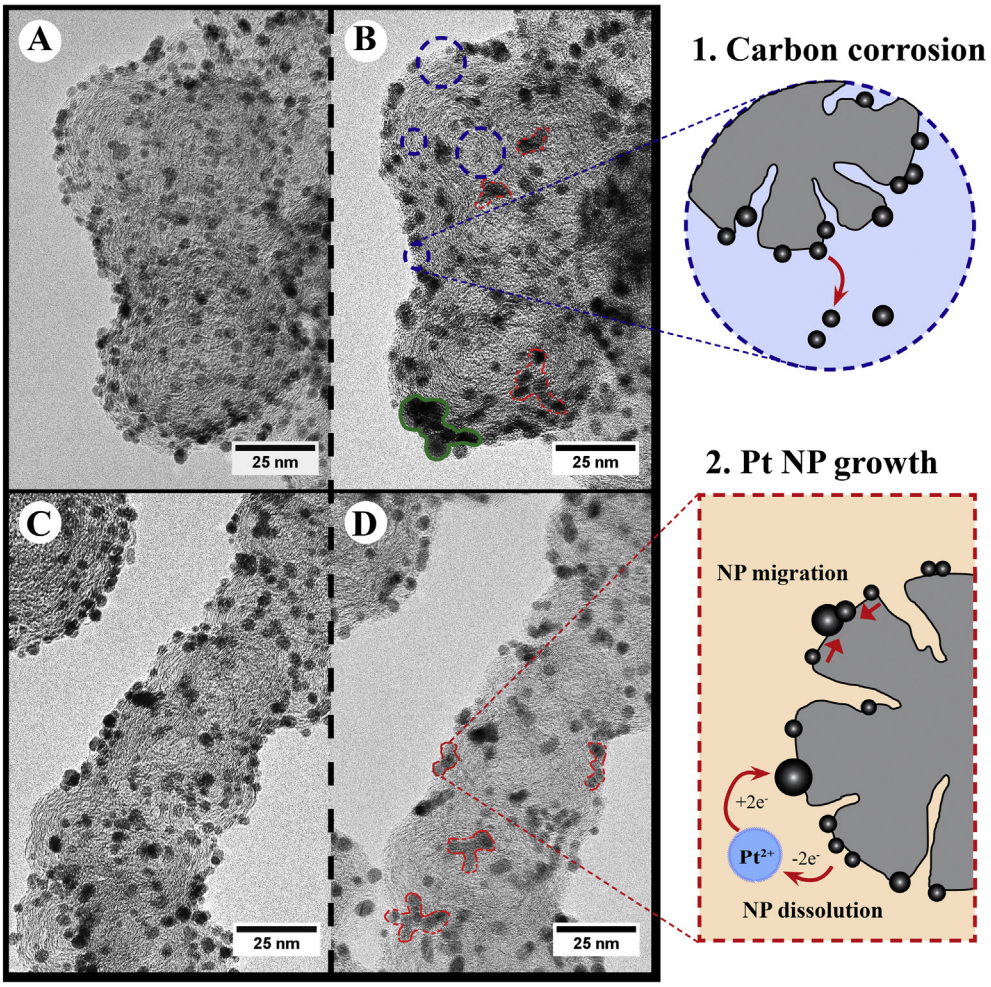

Fig. 4. IL-TEM micrographs of 30 wt. % Pt/Ketjenblack sample before and after AST protocols i.e. 27,000 potential cycles between 1.0 and 1.5 V_{RHE} with a sweep rate of 500 mV s^{-1} (A, B) and 9000 potential cycles between 0.6 and 1.0 V_{RHE} with a holding time of 3:3 s (C, D). The regions highlighted by colour are discussed in the text.

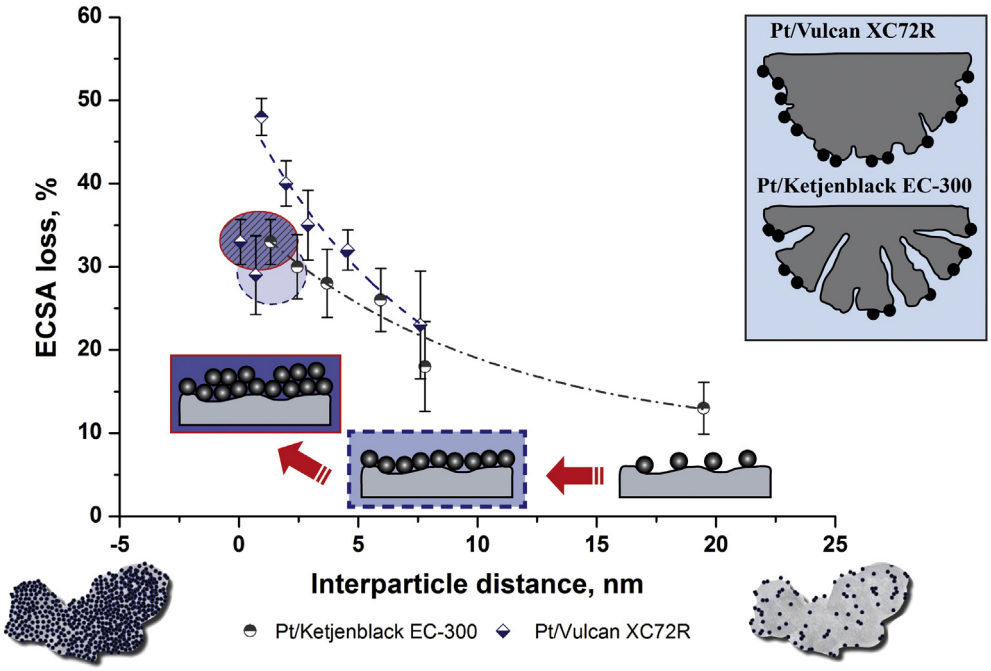

Fig. 5. Summary of the ECSA loss as function of interparticle distance (edge to edge) for Pt/Ketjenblack EC-300J and Pt/Vulcan XC72R samples after Start–Stop cycle treatment (15 h, 27,000 cycles). The highlighted areas indicate the data points where the catalysts exhibit Pt film behaviour.

dependence between the ECSA loss and the Pt loading is observed. Furthermore the carbon support exhibits only small influence as well.

In the following we therefore concentrate on Start–Stop conditions. In order to demonstrate that the support dependence is not solely determined by the surface area of the carbon support, in Fig. 5 we plotted the ECSA loss observed for Pt/Vulcan and Pt/Ketjenblack as a function of the interparticle distance. As interparticle distance we define the average distance between the edge of a Pt NP and the edge of its nearest neighbouring Pt NP [42]. If the synthesis method results in a loading independent particle size, as is the case here, the interparticle distance can be calculated based on the external BET surface area of the carbon support, the Pt loading and the average particle size of the Pt nanoparticles derived from TEM and SAXS measurements.

The data show that the behaviour of two carbons, Vulcan and Ketjenblack is not determined by their surface area alone, but that the carbon corrosion on Vulcan is enhanced due to a large number of defect sites [34]. The general trend of increasing ECSA loss with increasing Pt loading could be interpreted due to a catalytic effect of Pt NPs on carbon corrosion. An alternative explanation supported by a recent Raman study [33] could be a statistical factor. That is, increasing the number of Pt NPs that reside on a C flake enhances the likelihood of their detachment if the carbon flakes corrodes. Independent on the model, very high Pt to C ratios lead to a decrease in carbon corrosion. In order to characterize the behaviour of the Pt/C catalysts, we have to distinguish three cases: i) low to intermediate Pt loading; the carbon flakes are only partly covered by Pt NPs. ii) high Pt loading; the carbon flakes are fully covered by Pt NPs, yet no or minimal nanoparticle agglomeration is observed. The stability behaviour turns to that of a nanostructured Pt film. It seems the Pt NPs protect excessive carbon corrosion thus mitigating the corrosion rates. iii) Increasing the loading further, the properties of a nanostructured Pt film are kept, however, the Pt NPs agglomerate. Thus the Pt is insufficiently utilized.

Acknowledgements

This work was supported by the Danish DFF through grant no. 10-081337. We thank Dipl. Ing. Andrea Mingers of the group of Dr. Karl J.J. Mayrhofer at the MPIE for the ICP-MS analysis. We acknowledge the group of Prof. M. Bäumer (University of Bremen) for the collaboration concerning the NP synthesis.

References

[1] H.A. Gasteiger, N.M. Markovic, Science 324 (2009) 48–49.
[2] V.R. Stamenkovic, B. Fowler, B.S. Mun, G. Wang, P.N. Ross, C.A. Lucas, N.M. Markovic, Science 315 (2007) 493–497.
[3] J. Greeley, I.E.L. Stephens, A.S. Bondarenko, T.P. Johansson, H.A. Hansen, T.F. Jaramillo, J. Rossmeisl, I. Chorkendorff, J.K. Norskov, Nat. Chem. 1 (2009) 552–556.
[4] K.J.J. Mayrhofer, K. Hartl, V. Juhart, M. Arenz, J. Am. Chem. Soc. 131 (2009) 16348–16349.
[5] K.J.J. Mayrhofer, M. Arenz, Nat. Chem. 1 (2009) 518–519.
[6] K.J.J. Mayrhofer, J.C. Meier, S.J. Ashton, G.K.H. Wiberg, F. Kraus, M. Hanzlik, M. Arenz, Electrochem. Commun. 10 (2008) 1144–1147.
[7] K.J.J. Mayrhofer, S.J. Ashton, J.C. Meier, G.K.H. Wiberg, M. Hanzlik, M. Arenz, J. Power Sources 185 (2008) 734–739.
[8] F.S. Saleh, E.B. Easton, J. Electrochem. Soc. 159 (2012) B546–B553.
[9] F.S. Saleh, E.B. Easton, J. Power Sources 246 (2014) 392–401.
[10] S.J. Ashton, M. Arenz, J. Power Sources 217 (2012) 392–399.
[11] S.J. Ashton, M. Arenz, Electrochem. Commun. 13 (2011) 1473–1475.
[12] K. Hartl, M. Hanzlik, M. Arenz, Energy Environ. Sci. 4 (2011) 234–238.
[13] K. Schlogl, M. Hanzlik, M. Arenz, J. Electrochem. Soc. 159 (2012) B677–B682.
[14] Y. Wang, J.W. Ren, K. Deng, L.L. Gui, Y.Q. Tang, Chem. Mater. 12 (2000) 1622–1627.
[15] J. Speder, L. Altmann, M. Roefzaad, M. Baumer, J.J.K. Kirkensgaard, K. Mortensen, M. Arenz, Phys. Chem. Chem. Phys. 15 (2013) 3602–3608.
[16] A. Ohma, K. Shinohara, A. Iiyama, T. Yoshida, A. Daimaru, ECS Trans. 41 (2011) 775–784.
[17] J. Speder, A. Zana, I. Spanos, J.J.K. Kirkensgaard, K. Mortensen, M. Arenz, Electrochem. Commun. 34 (2013) 153–156.
[18] S.M.S. Kumar, J.S. Herrero, S. Irusta, K. Scott, J. Electroanal. Chem. 647 (2010) 211–221.
[19] K.J.J. Mayrhofer, G.K.H. Wiberg, M. Arenz, J. Electrochem. Soc. 155 (2008) P1–P5.
[20] K.J.J. Mayrhofer, S.J. Ashton, J. Kreuzer, M. Arenz, Int. J. Electrochem. Sci. 4 (2009) 1–8.

[21] H.A. Gasteiger, N. Markovic, P.N. Ross, E.J. Cairns, J. Phys. Chem. 98 (1994) 617–625.
[22] C.A. Reiser, L. Bregoli, T.W. Patterson, J.S. Yi, J.D.L. Yang, M.L. Perry, T.D. Jarvi, Electrochem. Solid State Lett. 8 (2005) A273–A276.
[23] Y.-C. Park, K. Kakinuma, M. Uchida, D.A. Tryk, T. Kamino, H. Uchida, M. Watanabe, Electrochim. Acta 91 (2013) 195–207.
[24] A. Ohma, K. Shinohara, A. Iiyama, T. Yoshida, A. Daimaru, in: H.A. Gasteiger, A. Weber, S.R. Narayanan, D. Jones, P. Strasser, K. SwiderLyons, F.N. Buchi, P. Shirvanian, H. Nakagawa, H. Uchida, S. Mukerjee, T.J. Schmidt, V. Ramani, T. Fuller, M. Edmundson, C. Lamy, R. Mantz (Eds.), Polymer Electrolyte Fuel Cells, vol. 11, 2011, pp. 775–784.
[25] D.A. Stevens, S. Zhang, Z. Chen, J.R. Dahn, Carbon 41 (2003) 2769–2777.
[26] E. Antolini, Appl. Catal. B 88 (2009) 1–24.
[27] G.G. Park, T.H. Yang, Y.G. Yoon, W.Y. Lee, C.S. Kim, Int. J. Hydrogen Energy 28 (2003) 645–650.
[28] S. Vengatesan, H.-J. Kim, S.-K. Kim, I.-H. Oh, S.-Y. Lee, E. Cho, H.Y. Ha, T.-H. Lim, Electrochim. Acta 54 (2008) 856–861.
[29] M. Uchida, Y. Fukuoka, Y. Sugawara, N. Eda, A. Ohta, J. Electrochem. Soc. 143 (1996) 2245–2252.
[30] Y. Takasu, T. Kawaguchi, W. Sugimoto, Y. Murakami, Electrochim. Acta 48 (2003) 3861–3868.
[31] X. Yu, S. Ye, J. Power Sources 172 (2007) 133–144.
[32] C. Prado-Burguete, A. Linares-Solano, F. Rodríguez-Reinoso, C.S.-M. de Lecea, J. Catal. 115 (1989) 98–106.
[33] A. Zana, J. Speder, N.E.A. Reeler, T. Vosch, M. Arenz, Electrochim. Acta 114 (2013) 455–461.
[34] M. Hara, M. Lee, C.-H. Liu, B.-H. Chen, Y. Yamashita, M. Uchida, H. Uchida, M. Watanabe, Electrochim. Acta 70 (2012) 171–181.
[35] M. Uchida, Y.-C. Park, K. Kakinuma, H. Yano, D.A. Tryk, T. Kamino, H. Uchida, M. Watanabe, Phys. Chem. Chem. Phys. 15 (2013) 11236–11247.
[36] A. Zana, J. Speder, M. Roefzaad, L. Altmann, M. Bäumer, M. Arenz, J. Electrochem. Soc. 160 (2013) F608–F615.
[37] M. Inaba, ECS Trans. 25 (2009) 573–581.
[38] S. Maass, F. Finsterwalder, G. Frank, R. Hartmann, C. Merten, J. Power Sources 176 (2008) 444–451.
[39] F.N. Büchi, M. Inaba, T.J. Schmidt, Polymer Electrolyte Fuel Cell Durability, Springer, New York, 2009.
[40] M. Cai, M.S. Ruthkosky, B. Merzougui, S. Swathirajan, M.P. Balogh, S.H. Oh, J. Power Sources 160 (2006) 977–986.
[41] R.L. Borup, J.R. Davey, F.H. Garzon, D.L. Wood, M.A. Inbody, J. Power Sources 163 (2006) 76–81.
[42] M. Nesselberger, M. Roefzaad, R. Faycal Hamou, P. Ulrich Biedermann, F.F. Schweinberger, S. Kunz, K. Schloegl, G.K.H. Wiberg, S. Ashton, U. Heiz, K.J.J. Mayrhofer, M. Arenz, Nat. Mater. 12 (2013) 919–924.